The Thesis Committee for Nora Jean Colligan
Certifies that this is the approved version of the following thesis:

Investigation of Lithium Cobalt Oxide Under Oxygen Evolution Reaction Conditions

APPROVED BY
SUPERVISING COMMITTEE:

Supervisor:

Arumugan Manthiram, Supervisor

Gyeong Hwang

Investigation of Lithium Cobalt Oxide Under Oxygen Evolution Reaction Conditions

by

Nora Jean Colligan, B.S. Mat Sci En

Thesis

Presented to the Faculty of the Graduate School of

The University of Texas at Austin

in Partial Fulfillment

of the Requirements

for the Degree of

Master of Science in Engineering

The University of Texas at Austin

May 2015

Dedication

I would like to thank my advisor, Professor Arumagan Manthiram, for allowing me to continue my education in his research group. I would also like to thank Professor Gyeong Hwang for taking the time to be my thesis reader. I am indebted to Dr. Veronica Augustyn for taking the time to show me how to prepare samples and run the electrochemical tests. Finally, I thank my family and friends for their support during my graduate education.

Abstract

Investigation of Lithium Cobalt Oxide Under Oxygen Evolution Reaction Conditions

Nora Jean Colligan, M.S.E.

The University of Texas at Austin, 2015

Supervisor: Arumugan Manthiram

Metal-air batteries are drawing much attention as the active material, O_2, could be directly used from air. The fundamental electrochemical reactions occurring in metal-air batteries are the oxygen reduction reaction (ORR) and oxygen evolution reaction (OER), which require the use of efficient catalysts to lower the overpotential and improve the efficiency. Many less expensive oxide catalysts are gaining much attention, but the mechanisms involved are still not well understood.

The electrocatalytic OER performance of various forms of lithium cobalt oxide has been studied to systematically establish the surface level catalytic mechanisms. The low-temperature lithiated spinel form of $LiCoO_2$ (designated as LT-$LiCoO_2$) exhibits lower overpotentials than the high-temperature layered form of $LiCoO_2$ (designated as HT-$LiCoO_2$), but this is shown to be a result of the increased surface area afforded by the lower-temperature synthesis conditions. Raman spectroscopy, along with the presence of an irreversible peak during the first cycle of the OER, demonstrates that the mechanism

for OER is the same for both the forms of $LiCoO_2$. At the surface level, lithium is removed during the first cycle of the OER, forming Co_3O_4 on the surface, which is likely the active site during the OER. This work highlights the importance of determining the nature of the catalyst surface when investigating the electrocatalytic properties of bulk materials.

Table of Contents

List of Tables

List of Figures

Chapter 1: Introduction

1.1 Motivation and Background

Increasing energy demands, global warming, and oil price fluctuations have emphasized the critical need for improved alternative energy storage and conversion technologies. Alternative energy conversion and storage devices can cleanly convert alternative energy sources to usable energy and store the produced electricity. Both types of devices have many active areas of research in order to provide cleaner sources and storage of energy for the future. Energy storage devices play a significant role in providing a stable supply of renewable energy with applications such as portable devices, transportation, and grid storage. Different applications have unique requirements in terms of safety, specific energy, specific power, cycle life, and cost.

Lithium-ion batteries have revolutionized the portable electronics market. However, the limited energy density based on insertion-compound electrodes, high cost, and safety concerns pose serious concerns for large applications, such as electric vehicles and grid storage.[1] Alternative battery technologies that could overcome some of these challenges are being explored, as shown in **Figure 1.1** below.

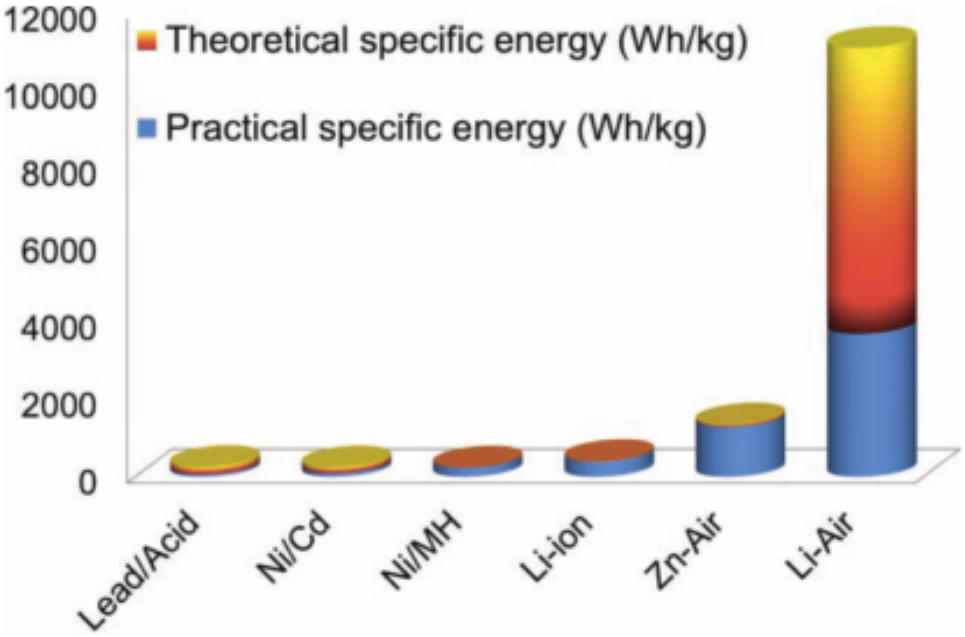

Figure 1.1 Theoretical and practical specific energies of various types of rechargeable batteries. Reprinted from ref [2].

Specifically, metal air batteries (Zn-air and Li-air) have attracted recent attention due to their high theoretical specific energies, which rival the theoretical specific energy of gasoline (13,000 Wh/kg).[3] The high theoretical specific energies are achievable because the active O_2 cathode material is not contained within the battery, while practical specific energies take into consideration the addition of functional materials required to operate the battery. Metal-air batteries are still under development with many technical challenges to overcome before they can be realized in practical cells.

1.2 METAL AIR BATTERIES

1.2.1 Design and Operating Principles

Metal-air batteries operate with a metal anode, an ion-conducting electrolyte, and a porous carbon air cathode. During discharge, the metal anode is oxidized while oxygen is reduced at the porous carbon cathode. Recharging the battery requires the reverse reactions to occur, and oxygen must be evolved at the air cathode. The electrochemical oxygen reduction reaction (ORR) and oxygen evolution reaction (OER) are a fundamental and, often times, limiting aspect of several clean-energy electrochemical technologies, including water electrolyzers, fuel cells, and metal-air batteries.[4]

One of the greatest challenges for metal-air batteries is the low round-trip charge/discharge efficiency due sluggish reaction kinetics and large overpotentials of the ORR and OER that occur at the air cathode during, respectively, discharge and charge.[4] **Figure 1.2** below demonstrates the inefficiencies as a result of the large overpotentials (η) of a typical charge and discharge curve for a Li-O_2 battery.[3] The oxygen evolution reaction, involved in charging the battery, has the highest overpotential and will be the focus of this study.

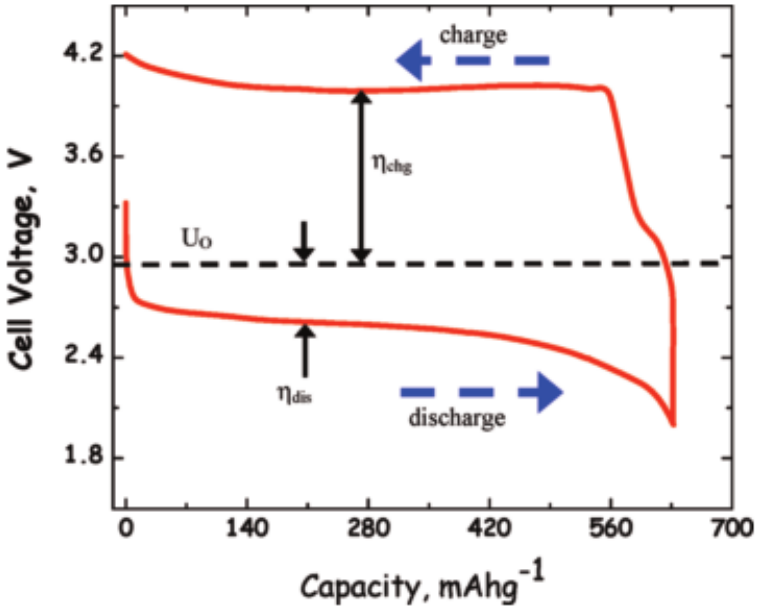

Figure 1.2 Sample discharge and charge curves for a Li-O_2 battery. Reprinted from ref [3].

Metal-air batteries with a lithium-metal anode have attracted recent attention because of their high theoretical specific energy density relative to lithium-ion batteries.[1] These lithium-air batteries have been studied in a number of different configurations as shown below in **Figure 1.2**.[2] This study will focus on the use of an alkaline aqueous electrolyte configuration.

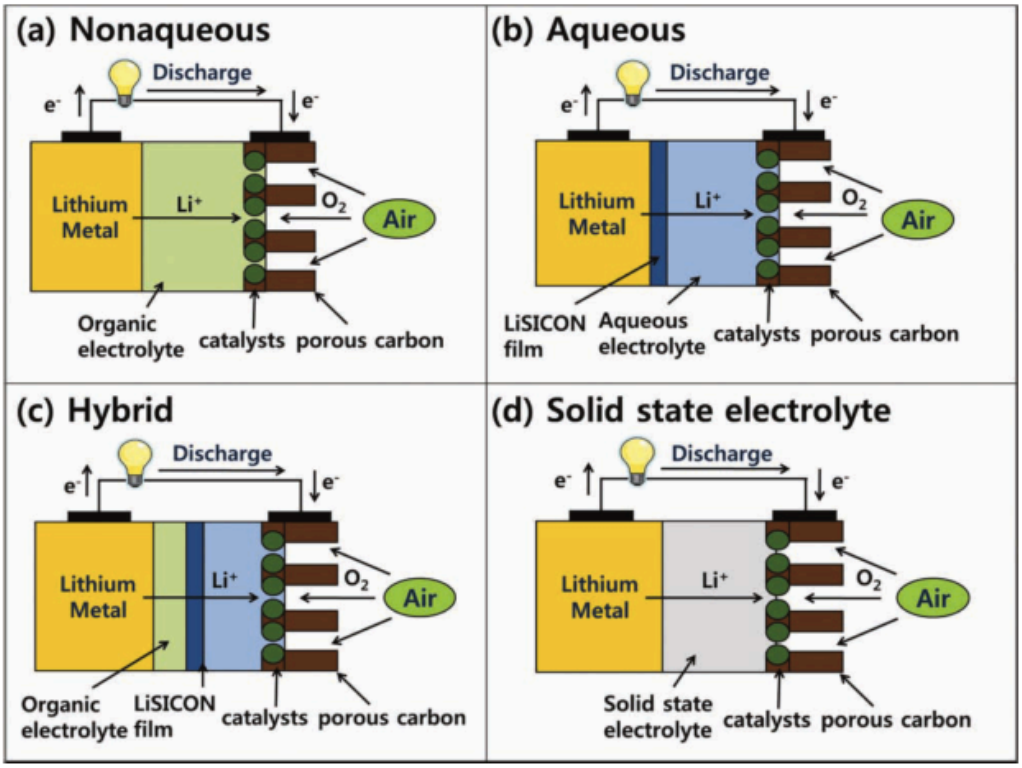

Figure 1.3 Schematics of cell configurations for the four types of Li-air batteries. Reprinted from ref [2].

Under aqueous alkaline conditions, the overall cell reaction for the Li – air battery is:[5]

$$2Li + \tfrac{1}{2}O_2 + H_2O \rightarrow 2LiOH \qquad E^o = 2.12 \text{ V vs. SHE}$$

During charging, the ideal four-electron OER at the cathode is:[5]

$$4OH^- \rightarrow O2 + 2H_2O + 4e^- \qquad E^o = 0.401 \text{ V vs. SHE}$$

In real systems, the OER occurs in a series of steps involving absorption and desorption of various species on the catalyst surface.[6] Several studies have focused on understanding the series of reactions and the kinetics involved with specific materials.[6–9] Understanding the complexities and rate limiting steps in OER is vital to lowering the overpotential of the charging step in metal-air batteries, so the study and development of catalyst materials has become a major focus of research in recent years.

1.2.2 OER Materials

Several different classes of catalyst materials, including noble metals, noble-metal oxides, and other metal oxides[10,11] have been investigated as potential candidates to improve the kinetics of the OER. RuO_2 and IrO_2 have been identified as highly active OER catalysts.[5] However, these noble-metal oxides are expensive and rare, giving further motivation to the discovery of highly active earth-abundant catalysts. Various mechanisms have been proposed to explain the trends in OER catalytic activity in specific classes of materials.[5] However, there have been few examples of highly active catalyst materials found from first principles calculations, and there has been significant effort on correlating materials properties with catalytic activity. Recent findings include correlating the M-OH bond strength for hydroxides,[12,13] the e_g electron count of perovskite oxides,[4] and the M-O bond length[14] to high electrocatalytic activity for the OER in alkaline electrolytes.

Since the correlation of materials properties with catalytic activity remains an active area of research, efforts have been made to standardize the methodology and reporting of activities.[11,15] However, realistic comparisons between different studies remains a challenge because reporting activity for classes of materials with variable surface areas is challenging. Commonly reported methods include Brunauer, Emmett and Teller (BET) surface area, electrochemical surface area (ECSA), electrode geometric area, and oxide catalyst loading. While each of these methods offers a different perspective, none of them offers a complete understanding of the reactions on the surface level. This study will focus on the surface-level mechanisms of the OER.

1.3 METAL OXIDE CATHODE MATERIALS

Layered $LiMO_2$ oxides consist of layers of Li^+ ions between octahedrally coordinated metal-oxygen layers, in which M can be V, Cr, Fe, Co, and Ni. These layered oxide materials were first investigated for battery materials in the 1980[16] and later combined and patented[17,18] with a graphite anode and commercialized by Sony Corporation.[19] The layered structure of the cathode allows two-dimensional intercalation of the Li^+ ions between the octahedral metal oxides, enabling the battery to be repeatedly charged and discharged. Since commercialization, these layered materials have been thoroughly studied, characterized, and improved for lithium-ion battery applications.[20] At lower temperatures, these materials can also adopt a lithiated spinel-like structure when prepared by low-firing temperatures (≤ 400 ºC) or lithium extraction.[21,22] The spinel structure provides three-dimensional lithium intercalation and greater stability upon lithium extraction. [22]

This thesis focuses on the catalytic activity of these materials with a goal of finding new activity predictors and understanding the mechanisms for enhanced activity. In this study, we characterize one of the most recognized lithium-ion battery materials $LiCoO_2$, crystallizing in the layered and lithiated spinel structures, and their catalytic behavior for the OER. The material prepared at higher temperatures (~ 800 ºC) adopts the layered structure and is designated hereafter as HT-$LiCoO_2$. The material prepared at lower temperatures (~ 400 ºC) adopts the lithiated spinel structure and is designated hereafter as LT-$LiCoO_2$.

Chapter 2: Experimental Methods

2.1 Materials Synthesis

The high-temperature form of $LiCoO_2$ (HT-$LiCoO_2$) sample was prepared by a solid-state reaction by mixing stoichiometric amounts of Co_3O_4 and Li_2CO_3 and heating at 800 °C for 24 h. The low-temperature form of ($LiCoO_2$ LT-$LiCoO_2$) was prepared by mixing stoichiometric amounts of Co_3O_4 and Li_2CO_3 and heating at 400 °C for 7 days. All chemicals were used as received. Chemically delithiated samples were prepared under an argon atmosphere with a Schlenk line. 300 mg of LT- or HT-$LiCoO_2$ were stirred with a required amount of the NO_2BF_4 oxidizing agent and 15 mL of anhydrous acetonitrile for 48 h. Lithium was chemically extracted according to the following reaction:

$$LiCoO_2 + xNO_2BF_4 \rightarrow Li_{1-x}CoO_2 + NO_2 + LiBF_4$$

The amount of NO_2BF_4 used in the reaction was varied in order to achieve the desired level of lithium extraction. The resulting product was filtered, washed with 100 mL of acetonitrile to remove the $LiBF_4$ byproduct, and then dried in an air oven overnight at 100 °C.

2.2 Materials Characterization

2.2.1 Scanning Electron Microscopy

The surface morphology was observed with a FEI Quanta FEG 600 scanning electron microscope (SEM). Samples were prepared by pressing powder into carbon tape on the SEM sample stubs.

2.2.2 Inductively Coupled Plasma Optical Emission Spectroscopy

Inductively coupled plasma-optical emission spectroscopy (ICP-OES) was performed with a Varian 715 instrument to determine the lithium content in all samples. Samples were prepared by dissolving 25mg of powder in 0.25mL of HNO_3 and 2mL of HCl prior to diluting it in 200mL of de-ionized water. The ICP measures the ion concentrations by ionizing the samples, then separating and measuring the concentrations of each individual ion with mass spectroscopy.

2.2.3 X-Ray Diffraction

X-ray diffraction (XRD) patterns were collected on a Phillips Vertical X-ray diffractometer with Cu Kα radiation (λ = 1.548 Å). Diffraction peaks were compared against the JCPDS database to verify the composition and crystal structure. Crystallite sizes were calculated by the Scherrer equation with the JADE software.

2.2.4 Brunauer, Emmett and Teller (BET) Surface Area

BET surface area measurements were performed on a Quantachrome Instruments Autosorb iQ gas sorption analyzer with nitrogen. At least 500mg of powder was dried at 100 ºC in a vacuum oven overnight, then heated to 150 ºC for 2 hours prior to N_2 physisorption measurement.

2.2.4 Raman Spectroscopy

Raman spectroscopy data were collected with a Witec Alpha 300 micro-Raman confocal microscope with an Ar laser excitation (λ = 488 nm). Raman samples were

prepared by dispersing 25 mg of the sample in 5 mL of ethanol, ultrasonicating for 30 min, and drop casting 10 μ L onto a stainless steel sheet.

2.3 Electrochemical Characterization

2.3.1 Catalyst Ink Preparation

Catalyst inks were prepared by mixing 25 mg of the sample, 5 mg acetylene black conductive additive, and 116 μLNafion solution (LQ-1105; Ion Power, Inc.) in 3.5 mL of deionized water and 1.5 mL of isopropyl alcohol under sonication for 30 min. The inks were mixed with an ultrasonic processor for 60 s just prior to electrode casting. Electrodes were drop-cast onto a 5 mm diameter glassy carbon electrode (Pine Instruments) with 5 μL of the catalyst ink, and dried under an infrared heat lamp for several minutes. Sample surfaces were wet with electrolyte prior to immersion in the electrolyte to prevent any bubbles from forming on the surface.

2.3.2 Rotating Disk Electrode (RDE)

Electrochemical measurements were performed with a traditional three-electrode cell with 0.1 M KOH as the electrolyte. The electrolyte was prepared with 18.2 MΩ water and bubbled with high purity O2 for 30 min prior to electrochemical measurements to ensure a saturated O2 atmosphere. The reference electrode was a saturated calomel electrode (SCE) and the counter electrode was a platinum mesh. The glassy carbon working electrode was rotated at a speed of 1600 rpm for the OER measurements. Cyclic voltammetry measurements were taken at a rate of 10 mV s−1. OER samples for Raman spectroscopy were prepared in the same manner, except the working electrode was the

stainless steel sheet prepared above and it remained stationary during the electrochemical measurement.

2.3.3 Electrochemical Surface Area

In order to estimate the change in surface area after OER, ESCA measurements were taken in a 0.1 M KOH electrolyte between –0.05 and +0.05 V, at scan rates between 5 and 100 mV s–1. The surface area was calculated from the double layer capacitance (C_{DL}) measured.

Chapter 3: $LiCoO_2$ as an Electrocatalyst*

3.1 Introduction

Cobalt oxides have been well-studied for lithium-ion battery applications, but their catalytic properties and trends in metal-air batteries have only recently been actively pursued.[23–26] $LiCoO_2$ is known to form in two different structural modifications. While the sample prepared at the conventional high temperature of ~ 800 °C adopts the well-known layered structure (designated at HT-$LiCoO_2$), that synthesized at ~ 400 °C adopts a lithiated spinel structure (designated as LT-$LiCoO_2$) in which the Li^+ ions occupy the 16c octahedral sites and the Co^{3+} ions occupy the 16d octahedral sites of the spinel framework. Here, we present a comparison of the OER catalytic activities of the LT-$LiCoO_2$ and HT-$LiCoO_2$ in alkaline medium, particularly with an examination of the species formed on the surface. Our results demonstrate that while the two forms of $LiCoO_2$ exhibit different specific and gravimetric activities, ex situ Raman results indicate that the surface of both of these materials become spinel (Co_3O_4)-like during OER. Our work highlights the difference between bulk and surface structures, as well as the difficulty of comparing catalytic activities between materials with different surface areas.

3.2 Structural Characterization and Elemental Analysis

XRD patterns of HT-$LiCoO_2$ and the respective delithiated samples are shown in **Figure 3.1a**. The XRD patterns of LT-$LiCoO_2$ and the respective delithiated samples are

---

* N. Colligan, V. Augustyn, A. Manthiram, "Evidence of Localized Lithium Removal in Layered and Lithiated Spinel $Li_{1-x}CoO_2$ ($0 \le x \le 0.9$) under Oxygen Evolution Reaction Conditions," *J. Phys. Chem. C,* 2015, DOI: 10.1021/jp511176j.
N. Colligan carried out the experimental work. V. Augustyn provided assistance in experimental details. A. Manthiram supervised the project. All participated in the preparation of the manuscript

shown in **Figure 3.1b**, with the reference diffraction patterns indicated with vertical lines at the bottom of each figure.

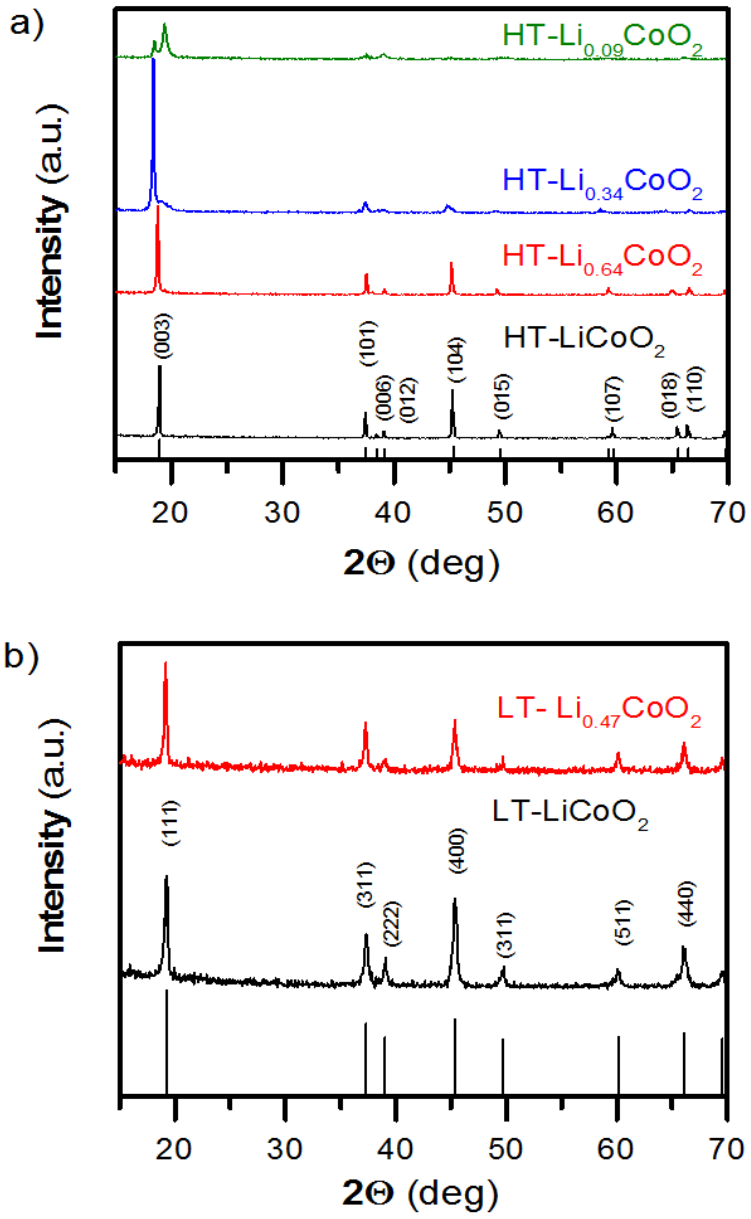

Figure 3.1 X-Ray diffraction patterns of (a) HT-$LiCoO_2$ and chemically delithiated HT-$Li_{1-x}CoO_2$ and (b) LT-$LiCoO_2$ and chemically delithiated LT-$Li_{1-x}CoO_2$.

The HT-$LiCoO_2$ sample in **Figure 3.1a** can be indexed to the space group $R\bar{3}m$ of layered $LiCoO_2$ (JCPDS # 00-062-0420). This well-known structure consists of alternating (111) planes of octahedrally coordinated Li^+ and Co^{3+} ions. The delithiated HT-$Li_{0.64}CoO_2$ sample maintains the layered structure, but when a significant amount of lithium is removed, as noted previously by our group[27] in $Li_{0.34}CoO_2$, the (003) peak at 18.96 ° develops a shoulder, indicating the phase transition from the O3 to the P1 structure. All the XRD patterns of the chemically de-lithiated samples are in alignment with previous work. The LT-$LiCoO_2$ sample in **Figure 3.1b** can be indexed to the space group Fd3m of cubic spinel (JCPDS #01-080-2159). Chemical extraction of 0.53 Li from LT-$LiCoO_2$ does not result in any apparent structural change from the XRD pattern. Previous studies by our group[22] show similar results, and also demonstrate that lithium moves from the 16d octahedral site to the 8a tetrahedral site in the spinel structure during de-lithiation. A decrease in lattice parameter is not observed because of the corresponding compensation from loss of oxygen from the lattice due to the overlap of the $Co^{3+/4+}$:3d band with the top of the O^{2-}:2p band.

The surface morphology of the HT-$LiCoO_2$ and LT-$LiCoO_2$ samples can be seen in **Figure 3.2**. The surface morphology of the as-fired HT-$LiCoO_2$ sample is composed of aggregates of ~ 2 μm rounded particles. The chemically de-lithiated samples show a more uniform size distribution of particles with much sharper edges as a result of stirring in acetonitrile and NO_2BF_4. The LT-$LiCoO_2$ samples show agglomerated particles, but differ from HT-$LiCoO_2$ due to the sub-micron primary particle size.

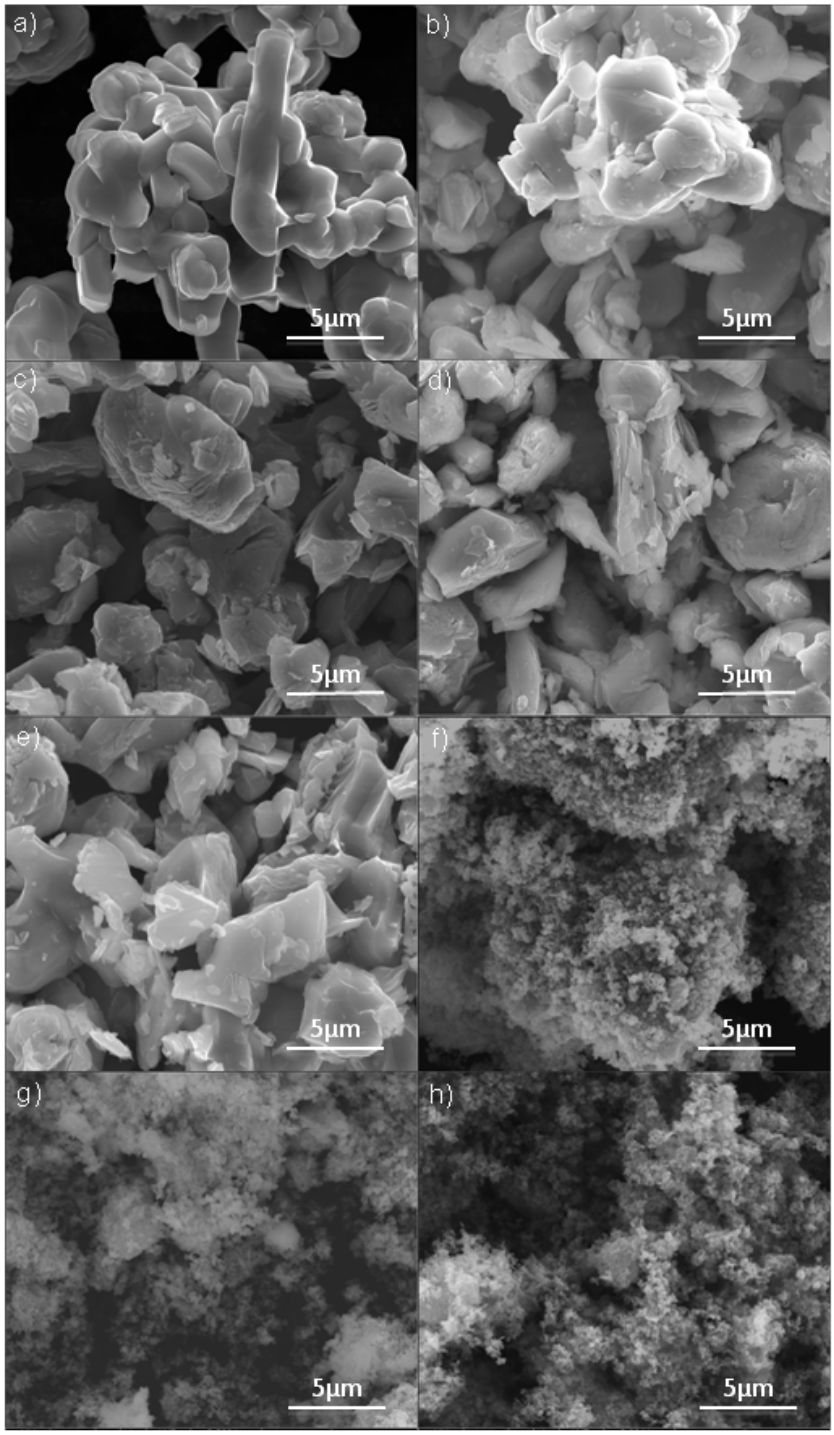

Figure 3.2 SEM images of (a) HT-$LiCoO_2$, (b) stirred HT-$LiCoO_2$, (c) HT-$Li_{0.64}CoO_2$, (d) HT-$Li_{0.34}CoO_2$, (e) HT-$Li_{0.09}CoO_2$, (f) LT-$LiCoO_2$, (g) stirred LT-$LiCoO_2$, and (h) LT-$Li_{0.47}CoO_2$.

The BET surface area measurements are summarized along with the primary particle and crystallite sizes in **Table 3.1** and are consistent with the SEM images. The low temperature sample has a higher surface area due to the lower firing temperature (400 vs. 800 °C). Samples stirred in acetonitrile and those that were chemically delithiated show similar primary particle sizes, but show increased surface damage and particle dispersion due to chemical treatment and stirring. The BET surface areas were used to normalize the electrochemical measurements.

Sample	BET Surface Area ($m^2 g^{-1}$)	Primary Particle Size (µm)	Crystallite Size (nm)
HT-$LiCoO_2$	0.4	~2	115
Stirred HT-$LiCoO_2$	1.9	~2	187
HT-$Li_{0.64}CoO_2$	4.4	~2	101
HT-$Li_{0.36}CoO_2$	3.2	~2	115
HT-$Li_{0.09}CoO_2$	3.1	~2	68
LT-$LiCoO_2$	1.2	~0.1	28
Stirred LT-$LiCoO_2$	15.2	~0.1	80
LT-$Li_{0.47}CoO_2$	18.9	~0.1	49

Table 3.1 BET surface area, SEM primary particle size, and crystallite size (from XRD) of the various $Li_{1-x}CoO_2$ samples.

3.3 Oxygen Evolution Reaction Catalytic Performance

The electrocatalytic activity of the samples for the OER was measured with cyclic voltammetry in an alkaline electrolyte. The normalization of electrocatalytic currents for materials of varying surface areas presents a challenge. Using oxide loading as a normalization factor represents the true amount of catalyst deposited on the electrode, but with varying particle size or morphology, the surface area may play a role in the activity.

Quantifying the activity by BET surface area also falls short of a perfect solution because it does not take into account what amount of the surface area plays a role in the catalytic activity. **Figure 3.3** shows the activity at 0.65 V *vs*. SCE (as calculated from the second CV cycle) with respect to BET surface area (mA cm^{-2}_{oxide}) and by catalyst loading (mA mg^{-1}). Normalizing the OER activity to either the oxide catalyst loading or the surface area yields very different results. The LT-$LiCoO_2$ exhibits the highest mass activity at 0.65V *vs*. SCE, but when the same data are shown normalized to BET surface area, HT-$LiCoO_2$ shows higher activity. Because LT-$LiCoO_2$ is prepared at a lower temperature (400 °C) than HT-$LiCoO_2$ (800 °C), the particle size is much smaller, yielding a higher surface area and higher catalytic activity by weight. Additionally, the stirred LT-$LiCoO_2$ sample, with an even higher BET surface area than the parent sample, shows increased activity when normalized by catalyst loading, but when normalized to BET surface area shows decreased activity. This leads to the question of which normalization method is more accurate and furthermore, what is happening to the surface of these materials during the OER.

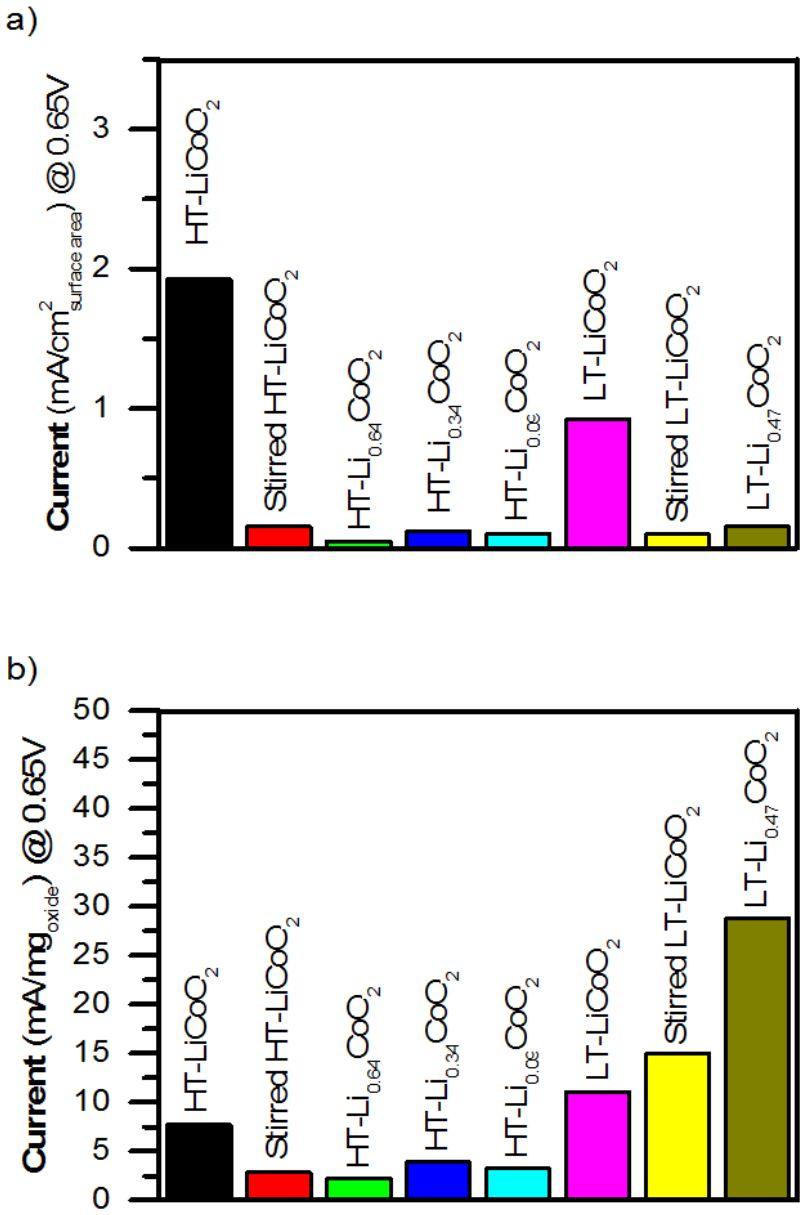

Figure 3.3 The OER activity of different $Li_{1-x}CoO_2$ samples at 0.65 V *vs*. SCE, taken from the second CV cycle: (a) normalized to the oxide's BET surface area and (b) normalized to catalyst mass loading.

To help explain the difference in activity trends we utilized ECSA analysis. ECSA is determined by obtaining the double layer capacitance (C_{DL}) by scanning across a small potential range in a non-faradic portion of the CV at varying scan rates. The double layer capacitance is related to surface area (*A*) by:

$$C_{DL} = \frac{\epsilon_R \epsilon_O A}{d}$$

where ϵ_R and ϵ_O are, respectively, the dielectric constants of the electrolyte and vacuum, and *d* is the thickness of the electrical double layer. While the above relationship is simple, in reality ECSA determination requires many assumptions, yielding large errors in the absolute values of the surface area.[11,28] Instead of focusing on absolute values, we studied the ESCA before and after OER cycling in order to better understand the surface conditions after oxygen evolution. Importantly, both HT-$LiCoO_2$ and LT-$LiCoO_2$ showed a ~ 9-fold increase in double layer capacitance after the OER, which should correlate to an increase in surface area. Representative CVs scanned at 10 mV s^{-1} can be found below in **Figure 3.4**. This large increase in surface area after the OER further indicates that the surface is transforming during the reaction, making normalization of activity to absolute surface area difficult.

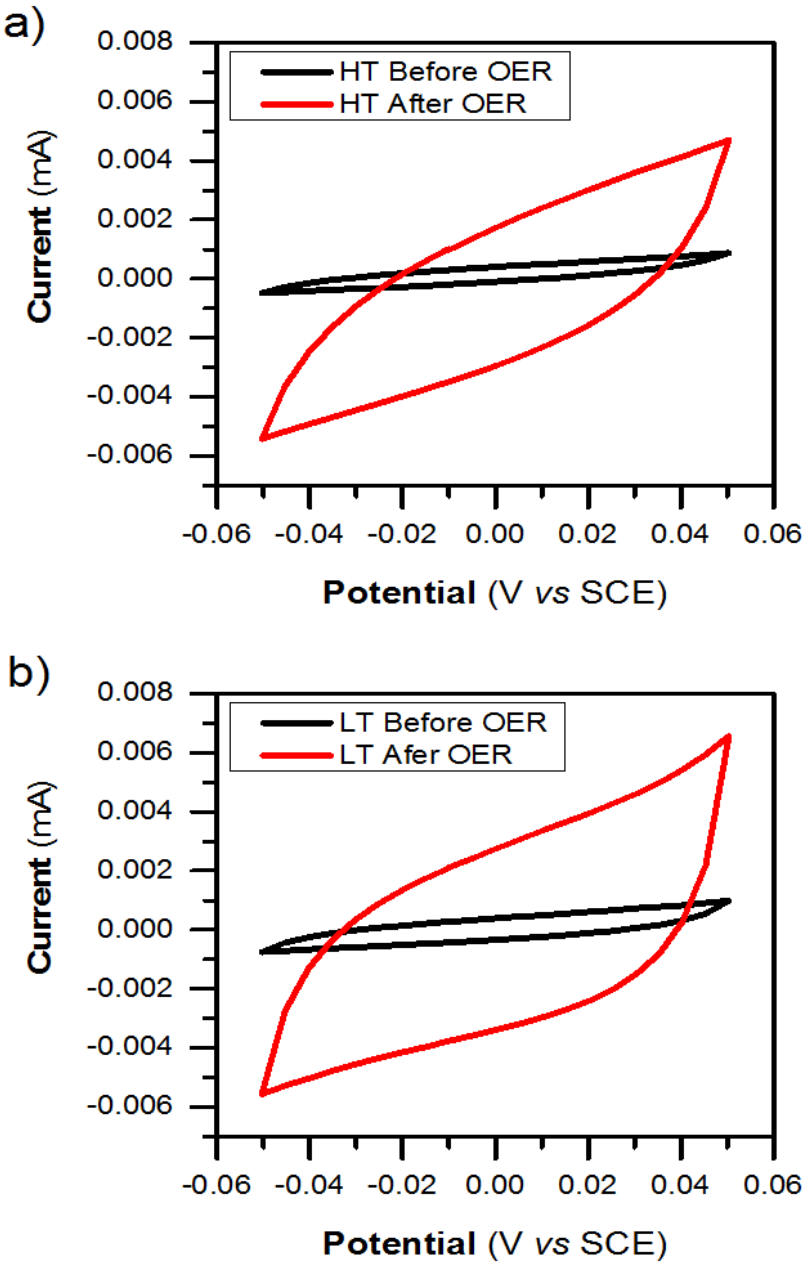

Figure 3.4 CVs of (a) HT-$LiCoO_2$ and (b) LT-$LiCoO_2$ in a non-faradaic region, showing the difference in double layer capacitance before and after OER.

Figure 3.5 shows the cyclic voltammograms (CVs) of HT-$Li_{1-x}CoO_2$ at a sweep rate of 10 mV s^{-1} and with a rotation rate of 1600 rpm. We can attempt to understand these surface level changes by first observing the differences between the first and second cycles of the OER, as shown in **Figures 3.5a** and **b**. The first cycle shows an irreversible anodic peak at ~ 0.5 V (*vs*. SCE) for LT-$LiCoO_2$ and at ~ 0.6 V for HT-$LiCoO_2$. This peak does not appear in the second cycle for either sample. The chemically delithiated samples do not exhibit this 1st-cycle irreversible peak, which has been ascribed to the extraction of Li^+ from the structure.[23,24]

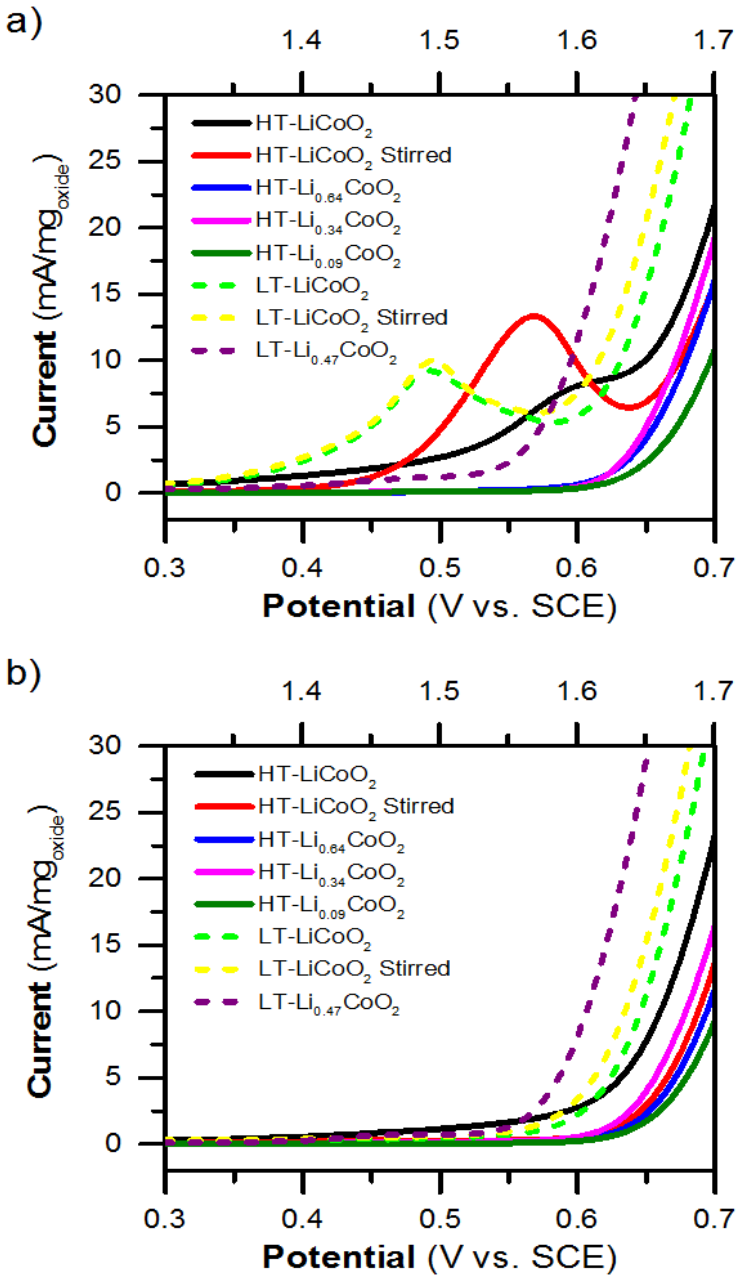

Figure 3.5 CVs of the $Li_{1-x}CoO_2$ at 10 mV s^{-1} in 0.1 M KOH: (a) first cycle and (b) 2nd cycle of the OER.

Based on the CV peak current, the amount of electrochemical delithiation corresponds to 0.12 Li from HT-$LiCoO_2$ and 0.11 Li from LT-$LiCoO_2$. While $LiCoO_2$ does exhibit

reversible Li^+ insertion in aqueous electrolytes,[29] in this work, the electrolyte does not contain Li^+ and so the delithiation process is irreversible. Lyons and Brandon previously published a detailed study of the surface reactions on cobalt metal, and discussed the complex nature of hydroxide attachment and oxide growth on Co^{3+} catalytic sites.[6] The CV results indicate that HT- and LT-$LiCoO_2$ undergo irreversible changes. To investigate these further, *ex situ* Raman spectroscopy was utilized to study the surface structure as it evolves during the OER reaction.

3.5 RAMAN SPECTROSCOPY

The vibrational modes of spinel (Fd3m) and layered ($R\bar{3}m$) $LiCoO_2$ can be determined from factor group analysis.[30] For the layered structure, these are the $A_{1g} + E_g + 2A_{2u} + 2E_u$, of which the A_{1g} and E_g bands are Raman-active. For the spinel structure, the vibrational modes are $A_{1g} + E_g + 2F_{2g} + 5F_{1u}$, of which the A_{1g}, E_g, and $2F_{2g}$ bands are Raman active.[31,32] Because of these site symmetry differences, we expect to see two Raman bands present in the layered HT-$LiCoO_2$ sample and four Raman bands in the spinel LT-$LiCoO_2$ sample. The Raman spectra of the as-prepared samples and the samples after OER cycles are shown in **Figure 3.6**.

The as-prepared HT-$LiCoO_2$ sample in **Figure 3.6a** clearly shows the two active Raman bands of the layered structure, at 485 and 595 cm^{-1}. The as-prepared LT-$LiCoO_2$ sample (**Figure 3.6b**) displays four Raman peaks at 446, 483, 588 and 600 cm^{-1}. These values agree quite well with the published values,[31] with only slight differences (< 10 cm^{-1}) seen in the LT-$LiCoO_2$ sample. After three cycles of the OER, new peaks emerge in the Raman spectrum of both HT- and LT-$LiCoO_2$. These peaks match well with the Raman spectra of Co_3O_4, which was recorded and shown for a reference at the bottom of

each plot. The Co_3O_4 spectra also agrees well with literature values of 194.4, 482.4, 521.6, 618.4, and 691.0 cm^{-1} for the Raman active modes of, respectively, F_{2g}, E_g, F_{2g}, F_{2g}, and A_{1g}.[33] The chemically delithiated HT-$Li_{0.64}CoO_2$ sample (**Figure 3.6c**), in the as-synthesized state, also exhibits Raman peaks attributed to Co_3O_4, even though the bulk structure consists of the layered phase, as evidenced by the XRD results of **Figure 3.1a**. This demonstrates that the Co_3O_4 phase is restricted to the surface of the materials. The Raman spectrum of the chemically delithiated LT-$Li_{0.47}CoO_2$ sample (**Figure 3.6d**) also contains peaks from both the spinel structure of LT-$LiCoO_2$ and Co_3O_4. After 10 OER cycles, all $Li_{1-x}CoO_2$ materials exhibit Co_3O_4 peaks in the Raman spectrum.

Previous transmission electron microscopy (TEM) studies[24,34] have shown evidence of surface transformations under OER conditions and electrochemical cycling. These studies show the appearance of an amorphous spinel-like phase on the surfaces, but do not offer insight into the composition of this phase. In addition, the presence of Co_3O_4 was found in $LiCoO_2$ thin films synthesized via pulsed laser deposition.[35] Raman evidence, along with the presence of the irreversible pre-OER peak in only the fully lithiated samples, establish that surface lithium removal is occurring during the first OER cycle, yielding a Co_3O_4 surface utilized in the subsequent cycles of OER.

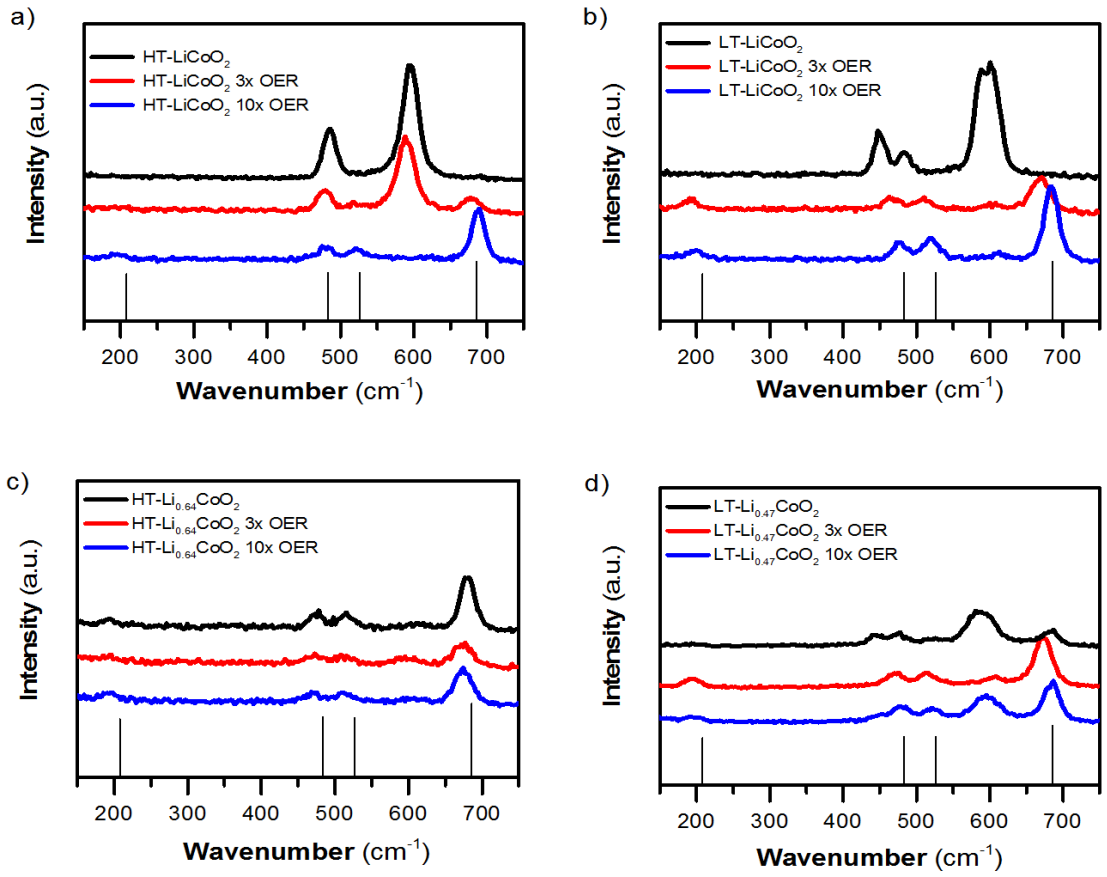

Figure 3.6 Raman spectra of the as-prepared samples and the samples after OER cycles: (a) HT-$LiCoO_2$, (b) LT-$LiCoO_2$, (c) HT-$Li_{0.64}CoO_2$, and (d) LT-$Li_{0.47}CoO_2$.

Chapter 4: Conclusion and Future Work

4.1 Conclusion

This study helps to establish the origin for the differences in the OER activity for different phases of $LiCoO_2$. The observed electrocatalytic activity of HT-$LiCoO_2$ compared to LT-$LiCoO_2$ differs based on the method of normalization due to differences in surface areas. A representative surface area is proven to be difficult to obtain due to the changing surface conditions during or after the OER. By studying the Raman spectra before and after OER, we establish that lithium removal occurs to form a Co_3O_4-like surface in both structures, and that the chemically-delithiated samples contain Co_3O_4 on the surface in the as-synthesized state. This agrees with the presence of an irreversible pre-OER peak in the CV during the first cycle and only in the case of the parent, lithiated cobalt oxides. Thus, the catalytic activity for OER for both forms of $LiCoO_2$ appears to be due to the presence of a Co_3O_4-like surface structure. This work highlights the importance of investigating the surface structure of bulk materials investigated for electrocatalysis.

4.2 Future Work

The detailed mechanism of the oxygen evolution reaction remains an elusive area of research and further systematic studies are needed in order to understand the surface level mechanisms. There are several classes of materials that show promising oxygen evolution reaction performance including nickel hydroxides,[36] nickel-iron oxides,[11,37] and cobalt oxides.[9] The origin of the enhanced OER activities of these materials is not well understood and further mechanistic studies of these materials will help enable the

development of predictors of enhanced activity. Development of these materials will be key to the future commercialization of the metal-air batteries.

References

(1) Bruce, P., Freunberger, S., Hardwick, L., Tarascon, J. Li – O 2 and Li – S Batteries with High Energy Storage. *Nat. Mater.* **2012**, *11*, 19–30.

(2) Lee, J. S.; Kim, S. T.; Cao, R.; Choi, N. S.; Liu, M.; Lee, K. T.; Cho, J. Metal-Air Batteries with High Energy Density: Li-Air versus Zn-Air. *Adv. Energy Mater.* **2011**, *1*, 34–50.

(3) Girishkumar, G.; Mccloskey, B.; Luntz, A. C.; Swanson, S.; Wilcke, W. Lithium - Air Battery : Promise and Challenges. **2010**, 2193–2203.

(4) Suntivich, J.; May, K. J.; Gasteiger, H. A.; Goodenough, J. B.; Shao-Horn, Y. A Perovskite Oxide Optimized for Oxygen Evolution Catalysis from Molecular Orbital Principles. *Science* **2011**, *334*, 1383–1385.

(5) Kinoshita, K. *Electrochemical Oxygen Technology*; Wiley: New York, 1992.

(6) Lyons, M. E. G.; Brandon, M. P. The Oxygen Evolution Reaction on Passive Oxide Covered Transition Metal Electrodes in Alkaline Solution Part II - Cobalt. *Int. J. Electrochem. Sci.* **2008**, *3*, 1425–1462.

(7) Lyons, M. E. G.; Brandon, M. P. The Oxygen Evolution Reaction on Passive Oxide Covered Transition Metal Electrodes in Aqueous Alkaline Solution . Part 1- Nickel. **2008**, *3*, 1386–1424.

(8) Matsumoto, Y.; Manabe, H.; Sato, E. Oxygen Evolution on La1− X Sr X CoO3 Electrodes in Alkaline Solutions. *J. Electrochem. Soc.* **1980**, *I*, 811–814.

(9) Zhu, J.; Ren, X.; Liu, J.; Zhang, W.; Wen, Z. Unraveling the Catalytic Mechanism of Co3O4 for the Oxygen Evolution Reaction in a Li-O2 Battery. *ACS Catal.* **2015**, *5*, 73–81.

(10) Jörissen, L. Bifunctional Oxygen/Air Electrodes. *J. Power Sources* **2006**, *155*, 23–32.

(11) McCrory, C. C. L.; Jung, S.; Peters, J. C.; Jaramillo, T. F. Benchmarking Heterogeneous Electrocatalysts for the Oxygen Evolution Reaction. *J. Am. Chem. Soc.* **2013**, *135*, 16977–16987.

(12) Rüetschi, P.; Delahay, P. Influence of Electrode Material on Oxygen Overvoltage: A Theoretical Analysis. *J. Chem. Phys.* **1955**, *23*, 556.

(13) Subbaraman, R.; Tripkovic, D.; Chang, K. C.; Strmcnik, D.; Paulikas, A. P.; Hirunsit, P.; Chan, M.; Greeley, J.; Stamenkovic, V.; Markovic, N. M. Trends in Activity for the Water Electrolyser Reactions on 3d M(Ni,Co,Fe,Mn) Hydr(oxy)oxide Catalysts. *Nat. Mater.* **2012**, *11*, 550–557.

(14) Trasatti, S. Electrocatalysis by Oxides - Attempt at a Unifying Approach. *J. Electroanal. Chem.* **1980**, *111*, 125–131.

(15) Suntivich, J.; Gasteiger, H. A.; Yabuuchi, N.; Shao-Horn, Y. Electrocatalytic Measurement Methodology of Oxide Catalysts Using a Thin-Film Rotating Disk Electrode. *J. Electrochem. Soc.* **2010**, *157*, B1263.

(16) Mizushima, K.; Jones, P. C.; Wiseman, P. J.; Goodenough, J. B. LixCoO2(O < X <= 1) - A New Cathode Material For Batteries Of High-Energy Density. *Mater. Res. Bull.* **1980**, *15*, 783–789.

(17) Nakajima; Yoshino, T.; Sanechika, A.; Kenichi. Secondary Battery. USP 4,668,595, 1985.

(18) A Yoshino, K Sanechika, T. N. Secondary Battery. Japanese Patent 1,989,293, 1985.

(19) Nagaura, T. in: *Progress In Batteries and Solar Cells*; JEC Press, Inc: Brunswick, OH, 1990; Vol. 9.

(20) Goodenough, J. B. Evolutions of Strategies for Modern Rechargeable Batteries. *Acc. Chem. Res.* **2013**, *46*, 1053–1061.

(21) Gummow, R. J.; Thackeray, M. M. Structure and Electrochemistry of Lithium Cobalt Oxide Synthesised at 400°C. *Mater. Res. Bull.* **1992**, *27*, 327–337.

(22) Choi, S.; Manthiram, A. Chemical Synthesis and Properties of Spinel Li1−xCo2O4−δ. *J. Solid State Chem.* **2002**, *164*, 332–338.

(23) Augustyn, V.; Manthiram, A. Characterization of Layered LiMO2 Oxides for the Oxygen Evolution Reaction of Metal-Air Batteries (M=Mn, Co, Ni). *Chempluschem* **2015**, *80*, 422–427.

(24) Lee, S. W.; Carlton, C.; Risch, M.; Surendranath, Y.; Chen, S.; Furutsuki, S.; Yamada, A.; Nocera, D. G.; Shao-Horn, Y. The Nature of Lithium Battery Materials under Oxygen Evolution Reaction Conditions. *J. Am. Chem. Soc.* **2012**, *134*, 16959–16962.

(25) Maiyalagan, T.; Jarvis, K. a; Therese, S.; Ferreira, P. J.; Manthiram, A. Spinel-Type Lithium Cobalt Oxide as a Bifunctional Electrocatalyst for the Oxygen Evolution and Oxygen Reduction Reactions. *Nat. Commun.* **2014**, *5*, 3949.

(26) Lu, Z.; Wang, H.; Kong, D.; Yan, K.; Hsu, P.-C.; Zheng, G.; Yao, H.; Liang, Z.; Sun, X.; Cui, Y. Electrochemical Tuning of Layered Lithium Transition Metal Oxides for Improvement of Oxygen Evolution Reaction. *Nat. Commun.* **2014**, *5*, 4345.

(27) Chebiam, R. V.; Prado, F.; Manthiram, a. Comparison of the Chemical Stability of Li1−xCoO2 and Li1−xNi0.85Co0.15O2 Cathodes. *J. Solid State Chem.* **2002**, *163*, 5–9.

(28) Trasatti, S.; Petrii, O. A. Real Surface Area Measurements in Electrochemistry. *Pure Appl. Chem.* **1991**, *63*, 711–734.

(29) Wang, G. J.; Qu, Q. T.; Wang, B.; Shi, Y.; Tian, S.; Wu, Y. P.; Holze, R. Electrochemical Behavior of LiCoO2 in a Saturated Aqueous Li2SO4 Solution. *Electrochim. Acta* **2009**, *54*, 1199–1203.

(30) Fateley, W. G.; McDevitt, N. T.; Bentley, F. F. Infrared and Raman Selection Rules for Lattice Vibrations: The Correlation Method. *Appl. Spectrosc.* **1971**, *25*, 155–173.

(31) Huang, W.; Frech, R. Vibrational Spectroscopic and Electrochemcial Studies of the Low and High Temperature Phases of LiCo1-xMxO2 (M=Ni or Ti). *Solid State Ionics* **1996**, *86-88*, 395–400.

(32) Kang, S. G.; Kang, S. Y.; Ryu, K. S.; Chang, S. H. Electrochemical and Structural Properties of HT-LiCoO 2 and LT- LiCoO 2 Prepared by the Citrate Sol-Gel Method. *Solid State Ionics* **1999**, *120*, 155–161.

(33) Hadjiev, V.; Iliev, M.; Vergilov, I. The Raman Spectra of Co3O4. *J. Phys. C Solid State Phys.* **1988**, *21*, 199–201.

(34) Wang, H.; Jang, Y.; Huang, B.; Sadoway, D. R.; Chiang, Y. TEM Study of Electrochemical Cycling-Induced Damage and Disorder in LiCoO 2 Cathodes for Rechargeable Lithium Batteries. *J. Electrochem. Soc.* **1999**, *146*, 473–480.

(35) Julien, C, Camacho-Lopez, M.A., Escobar-Alarcon, L, Haro-Poniatowski, E. Fabrication of LiCoO 2 Thin-Film Cathodes for Rechargeable Lithium Microbatteries. *Mater. Chem. Phys.* **2001**, *68*, 210–216.

(36) Song, F.; Hu, X. Exfoliation of Layered Double Hydroxides for Enhanced Oxygen Evolution Catalysis. *Nat. Commun.* **2014**, *5*, 1–9.

(37) Li, Y.; Selloni, A. Mechanism and Activity of Water Oxidation on Selected Surfaces of Pure and Fe-Doped NiOx. *ACS Catal.* **2014**, 4–9.